

# $K^-$ -Nucleus Scattering at Low and Intermediate Energies.

C. García-Recio, A.J. Melgarejo and J. Nieves

Departamento de Física Moderna, Universidad de Granada, E-18071 Granada, Spain.

## Abstract

We calculate  $K^-$ -nucleus elastic differential, reaction and total cross sections for different nuclei ( $^{12}\text{C}$ ,  $^{40}\text{Ca}$  and  $^{208}\text{Pb}$ ) at several laboratory antikaon momenta, ranging from 127 MeV (momentum of an antikaon produced in the  $\phi$ -meson decay) to 800 MeV. We use different antikaon-nucleus optical potentials, some of them fitted to kaonic atom data, and study the sensitivity of the results to the considered antikaon-nucleus dynamics. The possibility of using the scattering data to disentangle between different optical potentials, fitted to  $K^-$ -atom data, is discussed.

*PACS:* 13.75.Jz, 21.65.+f, 36.10.-k, 13.75.-n, 13.85.Dz, 11.30.Rd

*Keywords:* kaonic atoms and nuclei, antikaon nucleus scattering, chiral symmetry .

# 1 Introduction

In the last years there has been a renewed interest in the study of strangeness ( $S = -1$ ) meson-baryon systems. On one side, a lot of work has been devoted to the study of hypernuclei, from both the theoretical and experimental perspectives, greatly thanks to the new and precise measurements from KEK (see for instance Ref. [1]). On the other side, the pioneering works of Refs. [2, 3, 4] showed how Chiral Symmetry Constraints (CSC) could be accommodated within a unitarity approach, able to describe resonances, to the meson-baryon dynamics. This proved to be crucial to disentangle the intricate interaction between antikaons and nucleons at low energies<sup>1</sup> [5]–[8]. The model of Ref. [5], was used by Oset and Ramos to microscopically derive an optical potential for the  $K^-$  meson in nuclear matter in a self-consistent microscopic manner [9]. The approach used a  $s$ -wave  $\bar{K}N$  interaction obtained by solving a coupled-channel Bethe-Salpeter equation<sup>2</sup>, with a kernel determined by the lowest-order meson-baryon chiral Lagrangian. The approach followed by the authors of [5] restores exact unitarity and is able to accommodate the resonance  $\Lambda(1405)$ . Self-consistency turns out to be a crucial ingredient to derive the  $K^-$ -nucleus potential and leads to an optical potential considerably more shallow than those found in Refs. [14]–[18]. This was firstly pointed out by Lutz in Ref. [19], and also confirmed by the works of Refs. [20]–[21], where the medium modifications of antikaons in dense matter were studied in a coupled channel calculation, for scenarios more closely related to the environment of heavy-ion collisions.

In Refs. [22] and [23], the predictions of the theoretical potential developed in Ref. [9] for measured shifts and widths of kaonic atoms were evaluated. Some other phenomenological potentials, proposed in Refs. [15]–[18], were also examined in Ref. [23]. In that work, it is shown that the theoretical potential of Ref. [9], based on a chiral model, gives an acceptable description of the observed kaonic atom states through the whole periodic table<sup>3</sup>. Despite of having both real and imaginary parts of quite different depth, the empirical optical potentials used in Ref. [23] also led to acceptable descriptions of the experimentally available kaonic atom data. However, there were appreciable differences among the predicted widths for deeply bound antikaon nuclear states, not detected yet, when different potentials were used. Thus, the detection of such states would shed light on the intricacies of the antikaon behavior inside a nuclear medium. The depth of the real potential in the interior of nuclei is a topic of current interest in connection with possible kaon condensation in astrophysical scenarios [25].

The aim of this paper is to explore the possibility of differentiating between several antikaon nucleus optical potentials by means of the scattering data. The extrapolation to finite  $K^-$  kinetic energies of the potential of Ref. [9] requires at least the inclusion of the  $p$ -wave part of the antikaon selfenergy. This was performed in Ref. [24], where also the associated  $p$ -wave non-localities were studied at length.

---

<sup>1</sup>This reaction is specially complicated since the  $\Lambda(1405)$  resonance is placed quite close to the  $K^-p$  threshold.

<sup>2</sup>Similar extensions have been developed in the meson-meson sector [10]–[11] and also in the  $S = 0$  meson-baryon strangeness sector [12]–[13].

<sup>3</sup>This was also corroborated by the findings of Ref. [22].

However, even after having included  $p$ -wave contributions, one cannot expect reliable predictions from the theoretical potential of Refs. [9] and [24] at the lowest energy for which there are currently experimental data (800 MeV for the antikaon momentum in the laboratory frame). On the other hand, as we will show, for this relatively high energy, the impulse approximation works reasonably well, which is a clear indication that these data do not have much information on the details of the  $K^-$ -nucleus dynamics. Thus, we have also focused our attention at the typical momentum of antikaons after the  $\phi$ -meson decay ( $\approx 127$  MeV) with the hope that the scattering experience could be performed at DAΦNE or at KEK or in the future Japanese Hadron Collider (JHC).

The paper is organized as follows. In Sect. 2, basic definitions and normalizations of amplitudes and cross sections are given. There also the Klein Gordon Equation (KGE), which will be solved afterwards, is introduced. In Sect. 3 the different models for the antikaon-nucleus dynamics are examined. And, finally, in Sect. 4 we present our results and conclusions.

## 2 The Klein-Gordon Equation and the Elastic and Reaction Cross Sections

Because of the Coulomb interaction, the  $K^-$  kinetic energy inside the nucleus will differ from its asymptotical, far from the interaction region, value. The absorptive  $K^-$ -nucleus optical potential should depend on the antikaon kinetic energy, since it plays a major role in the evaluation of the phase space available. This effect proved to be quite important for  $\pi$ -nucleus scattering [26], and to take it into account for a laboratory energy  $\omega'$  of the antikaon we evaluate the strong potential,  $V_{\text{opt}}$ , in the point  $\vec{r}$  at an energy

$$T = \omega' - m - V_C(\vec{r}) \quad (1)$$

with  $m = 493.677$  MeV and  $V_C(\vec{r})$  the finite-size Coulomb potential, and then solve the KGE with the physical Center of Mass (CM) energy of the antikaon,  $\omega$ ,

$$\left( -\vec{\nabla}^2 + \mu^2 + 2\omega V_{\text{opt}} \right) \Psi = (\omega - V_C)^2 \Psi, \quad (2)$$

with  $\mu$  the reduced antikaon-nucleus mass. Asymptotically, Eq. (2) is equivalent to a Schrödinger equation where  $\omega$  plays the role of the mass and  $(\omega^2 - \mu^2)/2\omega$  plays the role of the non-relativistic energy. We solve numerically the KGE by means of an accurate method to solve the Schrödinger equation [27] which has been previously tested in the study of  $\pi$ -nucleus scattering [26]. The antikaon wave-function  $\Psi(\vec{r})$  behaves

$$\lim_{r \rightarrow \infty} \Psi(\vec{r}) \rightarrow I(r) + f(\theta)S(r) \quad (3)$$

with  $I(r)$  and  $S(r)$  the standard Coulomb wave functions [28] for Coulomb scattering from a punctual charge  $Z$ . The partial wave decomposition of the CM scattering amplitude reads:

$$f(\theta) = -\frac{i}{2q} \sum_{l=0}^{\infty} (2l+1) \left[ \eta e^{2i(\sigma_l + \delta_l)} - 1 \right] P_l(\cos(\theta)) \quad (4)$$

with  $\theta$  and  $q$  the scattering angle and momentum in the antikaon-nucleus CM frame,  $P_l$  Legendre polynomials,  $\sigma_l$  the standard Coulomb phase shift [28],  $\delta_l$  the additional phase shift due to strong interaction and  $\eta_l$  the inelasticity. The normalization of the scattering amplitude is determined by its relation to the differential elastic cross section in CM,

$$\frac{d\sigma_e}{d\Omega} = |f(\theta)|^2 \quad (5)$$

and finally the integrated cross sections read:

$$\sigma_e = \frac{\pi}{q^2} \sum_l (2l+1) \left| 1 - \eta_l e^{2i(\sigma_l + \delta_l)} \right|^2, \quad (6)$$

$$\sigma_{\text{tot}} = \frac{2\pi}{q^2} \sum_l (2l+1) [1 - \eta_l \cos(2(\sigma_l + \delta_l))], \quad (7)$$

$$\sigma_{\text{react}} = \frac{\pi}{q^2} \sum_l (2l+1) [1 - \eta_l^2] \quad (8)$$

While the elastic ( $\sigma_e$ ) and total ( $\sigma_{\text{tot}}$ ) cross sections are infinite, the reaction ( $\sigma_{\text{react}}$ ) cross section is finite because of the short-range of the nuclear interaction.

### 3 $K^-$ -Nucleus Optical Potentials:

The  $K^-$ -nucleus optical potential,  $V_{\text{opt}}$ , is related to the  $K^-$ -selfenergy,  $\Pi$ , inside of a nuclear medium. This relationship reads:

$$2\omega V_{\text{opt}}(r) = \Pi \left( q^0 = m + T, |\vec{q}| = \sqrt{q^0{}^2 - m^2}, \rho_p(r), \rho_n(r) \right), \quad (9)$$

where  $\rho_{p(n)}(r)$  is the proton (neutron) density. In what follows we will only refer to self-energies. Neglecting isovector effects, as we will do in the rest of the paper, the selfenergy only depends on  $\rho(r) = \rho_p(r) + \rho_n(r)$ . Charge densities are taken from [29]. For each nucleus, we take the neutron matter density approximately equal to the charge one, though we consider small changes, inspired by Hartree-Fock calculations with the DME (density-matrix expansion) [30]. In Table 1 we compile the densities used through this work. However charge (neutron matter) densities do not correspond to proton (neutron) ones because of the finite size of the proton (neutron). We take that into account following the lines of Ref. [32].

As we mentioned in the introduction, the authors of Ref. [9] have developed a complex selfenergy for the  $K^-$  meson in nuclear matter in a self-consistent microscopic manner. It is based on their previous work [5] on the  $s$ -wave meson-baryon dynamics in the  $S = -1$  strangeness sector, where CSC were incorporated. The results in nuclear matter are translated to finite nuclei by means of the local density approximation. The selfenergy evaluated in Ref. [9] consisted of  $s$ - and  $p$ -wave contributions. The  $s$ -wave part was quite complete, however the  $p$ -wave one was far from complete and only contains the

Nucleus	$R_p$ [fm]	$R_n$ [fm]	$a$ [fm]*
$^{12}\text{C}$	1.672	1.672	1.150
$^{40}\text{Ca}$	3.51	3.43	0.563
$^{208}\text{Pb}$	6.624	6.890	0.549

Table 1: Charge ( $R_p, a$ ) and neutron matter ( $R_n, a$ ) density parameters. For carbon we use a modified harmonic oscillator (MHO),  $\rho(r) = \rho_0(1 + a(r/R)^2) \exp(-(r/R)^2)$ , whereas for calcium and lead a two-parameter Fermi distribution,  $\rho(r) = \rho_0/(1 + \exp((r - R)/a))$ , was used. (\*) The parameter  $a$  is dimensionless for the MHO density form.

contributions of  $\Lambda$ -hole and  $\Sigma$ -hole excitations at first order. Later on, the  $p$ -wave part of the antikaon selfenergy was updated in Ref. [24] and tested for  $K^-p$  scattering in Ref. [31]. In Ref. [24], the  $\Sigma^*$ -hole excitation effects on the self-consistent determination of the  $s$ -wave  $K^-$  selfenergy were also included and found to be important (see Sect.6-2 of Ref. [24]). From the antikaon-selfenergy as determined by Refs. [9] and [24], we define, the first complex selfenergy used in this work ( $\Pi^{\text{TH}}$ ). This selfenergy does not have any free parameters, all the needed input is fixed either from studies of meson-baryon scattering in the vacuum or from previous studies of pionic atoms [32]. It provides a more than acceptable ( $\chi^2$  per number of datum of 2.9) description of the set of 63 shifts and widths of kaonic atom levels used in Ref. [23]. Non-local terms associated to the  $s$ -wave part of the selfenergy are negligible for kaonic atoms when they are properly dealt [24]. On the other hand, though non-localities might be important for the  $p$ -wave, this part of the theoretical potential represents only a correction to the dominant (local)  $s$ -wave part at low energies. The lower the antikaon momentum, the higher the non-local effects become, but even for the lowest laboratory antikaon momentum explored in this work ( $q = 127$  MeV), the inclusion of non-localities in the  $p$ -wave leads to changes of around 3% at most. Thus, all non-localities have been neglected, even in the  $p$ -wave contribution of the selfenergy, which has been treated as a local contribution, i.e, proportional to  $\vec{q}^2$  instead of the usual  $\vec{\nabla} \cdots \vec{\nabla}$  form.

In the spirit of Ref. [23], we also construct a modified selfenergy, which we call  $\Pi^{\text{THPH}}$ , by adding to  $\Pi^{\text{TH}}$  a phenomenological part linear in density. This phenomenological part is determined by a complex constant  $\delta b_0$  which we fix to the value obtained in Ref. [23] from a  $\chi^2$ -fit to the kaonic atom data. The new selfenergy reads:

$$\Pi^{\text{THPH}}(r) = \Pi^{\text{TH}}(r) - 4\pi \times \delta b_0 \rho(r) \quad (10)$$

with  $\delta b_0 = (0.12 - i 0.38)\text{fm}$ .

This new selfenergy,  $\Pi^{\text{THPH}}$ , for kaonic atoms ( $q^0 = m$ ) led to a better description [23] of shifts and widths than that the purely theoretical one,  $\Pi^{\text{TH}}$ . The semiphenomenological selfenergy,  $\Pi^{\text{THPH}}$ , has a larger attractive real part, and a smaller absorptive imaginary part than the totally theoretical one  $\Pi^{\text{TH}}$ . At threshold, for kaonic atom data, one might quantify these deficiencies by about 15% and 30% for the real and imaginary parts respectively [23]. Taking into account that the imaginary part of an optical potential provides

an effective repulsion [18] the semiphenomenological selfenergy is more attractive than  $\Pi^{\text{TH}}$ .

The third selfenergy considered in this work is just obtained from the Impulse Approximation (IA), i.e.,  $t\rho$  form for the antikaon selfenergy, where  $t$  is the elementary forward scattering amplitude of the antikaon with the nucleons, averaged over isospin and the Fermi motion of the nucleons. Such a model neglects all orders higher than the leading one in the density expansion. We will denote it by  $\Pi^{\text{IA}}$  and, neglecting all type of non-localities, reads:

$$\Pi^{\text{IA}}(r) = -4\pi \frac{\sqrt{s}}{M} \times b_0(\sqrt{s}) \rho(r) \quad (11)$$

$$b_0(\sqrt{s}) = \frac{1}{4} (3 {}_1 f(\sqrt{s}) + {}_0 f(\sqrt{s})) \quad (12)$$

with  $M = 938.27$  MeV the nucleon mass,  $\sqrt{s}$  the total CM antikaon-nucleon energy and  ${}_{I=1,0} f$  the isoscalar and isovector forward antikaon-nucleon scattering amplitude, with normalization such that the isospin  $I$  forward elastic differential cross section is just  $|{}_I f|^2$ . The partial wave decomposition of  ${}_I f$  reads [33]

$${}_I f(\sqrt{s}) = \sum_l \left( (l+1) {}_I f_l^{j=l+1/2}(\sqrt{s}) + l {}_I f_l^{j=l-1/2}(\sqrt{s}) \right) \quad (13)$$

with  $j$  the total angular momentum. It is well known that at threshold [34]

$$b_0(m+M) = (-0.15 + i 0.62) \text{ fm} \quad (14)$$

and with this value of  $b_0$ , the IA leads to quite poor results for kaonic atoms. Indeed best fit to the  $K^-$ -atom data provides [14],[23] values for  $b_0(m+M)$  with real parts about four times larger in modulus and opposite in sign that the value quoted above and obtained from the experimental scattering lengths. This is a clear indication that higher density corrections, not taken into account within the IA, are extremely important for kaonic atoms.

Finally, we have also considered two more local antikaon complex selfenergies fitted to the kaonic atom data and energy independent. We aim to compare them with those described up to now, only for small antikaon momenta, where one can assume that non-vanishing kinetic energies lead to moderate/small changes. These two new models are inspired in the works of Refs. [16] and [18] and read:

$$\Pi^{\text{IAPH}}(r) = -4\pi \left( 1 + \frac{\mu}{M} \right) \tilde{b}_0 \rho(r) \quad (15)$$

$$\Pi^{\text{2DD}}(r) = -4\pi \left( 1 + \frac{\mu}{M} \right) \rho(r) \left( b_0(m+M) + B_0 \left( \frac{\rho(r)}{\rho_0} \right)^\alpha \right) \quad (16)$$

with  $\tilde{b}_0 = (0.52 + i 0.80)$  fm,  $B_0 = (1.62 - i 0.028)$  fm and  $\alpha = 0.273$  as determined from  $\chi^2$ -fits to  $K^-$ -atom data in Ref. [23]. Note that  $\Pi^{\text{IAPH}}$  is just a phenomenological modification of the IA selfenergy  $\Pi^{\text{IA}}$ .

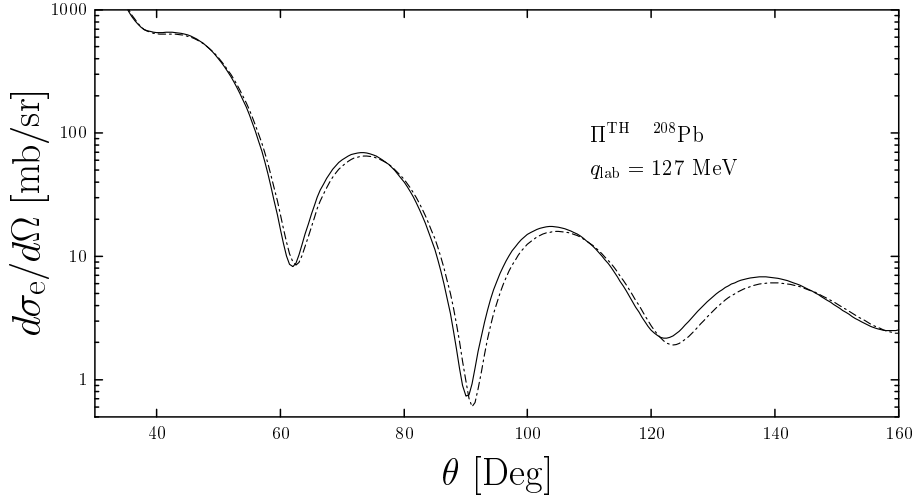


Figure 1: CM differential cross section for elastic scattering of  $q_{\text{lab}} = 127 \text{ MeV } K^-$  from  $^{208}\text{Pb}$  with the antikaon selfenergy  $\Pi^{\text{TH}}$ . The solid (dashed) line stands for the results when the Coulomb correction to the antikaon kinetic energy in Eq. (1) is not taken (is taken) into account.

## 4 Results and Concluding Remarks

Since the  $K^-$  lifetime is relatively small, in practical terms it is experimentally difficult to count with low energetic  $K^-$  beams. However, all selfenergies described in the previous section, except for that obtained in the IA, are valid only near threshold. Thus, we have studied the case  $q_{\text{lab}} = 127 \text{ MeV}$ , since this is the kaon momentum after the  $\phi$ -meson decay, with the hope that the corresponding scattering experience could be performed at DAΦNE or at KEK or in the next future at the JHC.

Firstly, we have studied the effect of correcting the kinetic energy of the antikaon due to the Coulomb attraction, as discussed in Eq. (1). Results for  $^{208}\text{Pb}$ , where we expect the higher effects, are shown in Fig. 1. As one can appreciate in the figure the variations in the CM differential elastic cross section are negligible and, in addition, the changes in the reaction cross section are just of the order of one per cent. Therefore, in what follows, we will not correct the antikaon kinetic energies.

Secondly, we have tested both for the variation of the Refs. [9] and [24] antikaon-nucleus dynamics when going from threshold to  $T = 16.1 \text{ MeV}$  (laboratory kinetic energy associated to  $q_{\text{lab}} = 127 \text{ MeV}$ ) and for the effect of the empirical  $\delta b_0$  term in  $\Pi^{\text{THPH}}$ . Results for scattering off  $^{12}\text{C}$  are shown in Fig. 2, where it can be seen that the antikaon selfenergy of the Refs. [9] and [24] evaluated at threshold or at  $T = 16.1 \text{ MeV}$  leads to small changes in the CM differential elastic cross section. Also the change in the reaction cross section is small and it represents only around a 3%. This is in agreement with

our previous result on the small effect of correcting the antikaon kinetic energy by the Coulombian potential.

However, the inclusion of the empirical  $\delta b_0$  term leads to more appreciable changes in the elastic cross section, though the variation of the reaction cross section is small (about 2%).

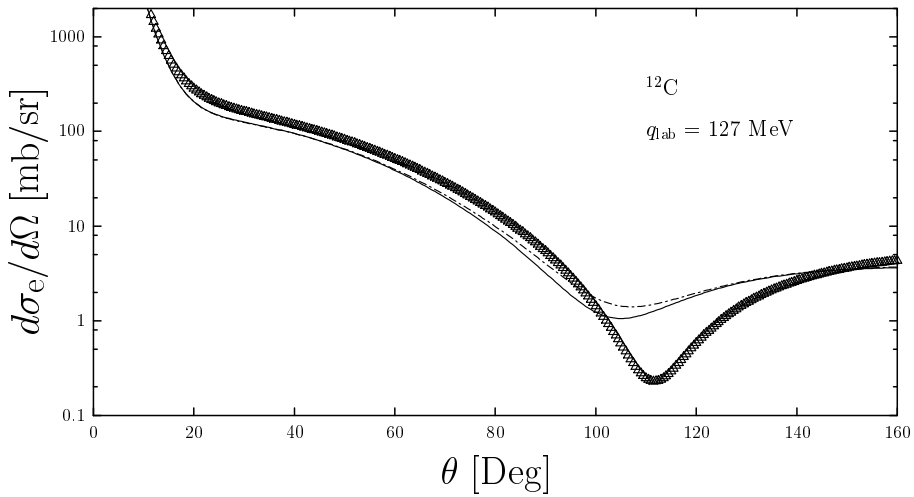


Figure 2: CM differential cross section for elastic scattering of  $q_{\text{lab}} = 127$  MeV  $K^-$  from  $^{12}\text{C}$  with different optical potentials. The solid line and the cross point line have been obtained with  $\Pi^{\text{TH}}$  and  $\Pi^{\text{THPH}}$  selfenergies respectively, while the dashed line has been obtained by using  $\Pi = \Pi^{\text{TH}}|_{q^0=m}$ .

Since the dynamics of the antikaon inside of the nuclear medium does not drastically change from threshold to  $T = 16.1$  MeV, at least for the theoretical model of Refs. [9] and [24], in Fig. 3 we also present results obtained with the complex antikaon selfenergies, fitted to the kaonic atom data, given in Eqs. (15) and (16). We also show results obtained by using the IA, where we have approximated the IA selfenergy at  $T = 16.1$  MeV by its threshold value quoted above (Eq. (14)). Strong interaction integrated elastic, reaction and total cross sections for all potentials of Fig. 3 are also given in Table 2. We obtain these cross sections after having got rid of the Coulombian interaction, otherwise the total and elastic cross sections would diverge, i.e., we compute strong phase-shifts and inelasticities ( $\delta_l$  and  $\eta_l$ ) in presence of the Coulomb interaction, and afterwards we set to zero the Coulombian phase shifts,  $\sigma_l$ , in the formulae of Eqs. (6)-(8). The first observation we would like to make is that the non-linear density dependent antikaon self-energy,  $\Pi^{2\text{DD}}$ , and the linear, in density, threshold IA selfenergy,  $\Pi(\sqrt{s}) = \Pi^{\text{IA}}|_{\sqrt{s}=m+M}$  provide extraordinarily similar results. Since both models have the same leading term in density, determined by the parameter  $b_0(m+M)$ , this is a clear indication that the reaction takes place in the surface of the nuclei, because of the big imaginary part of

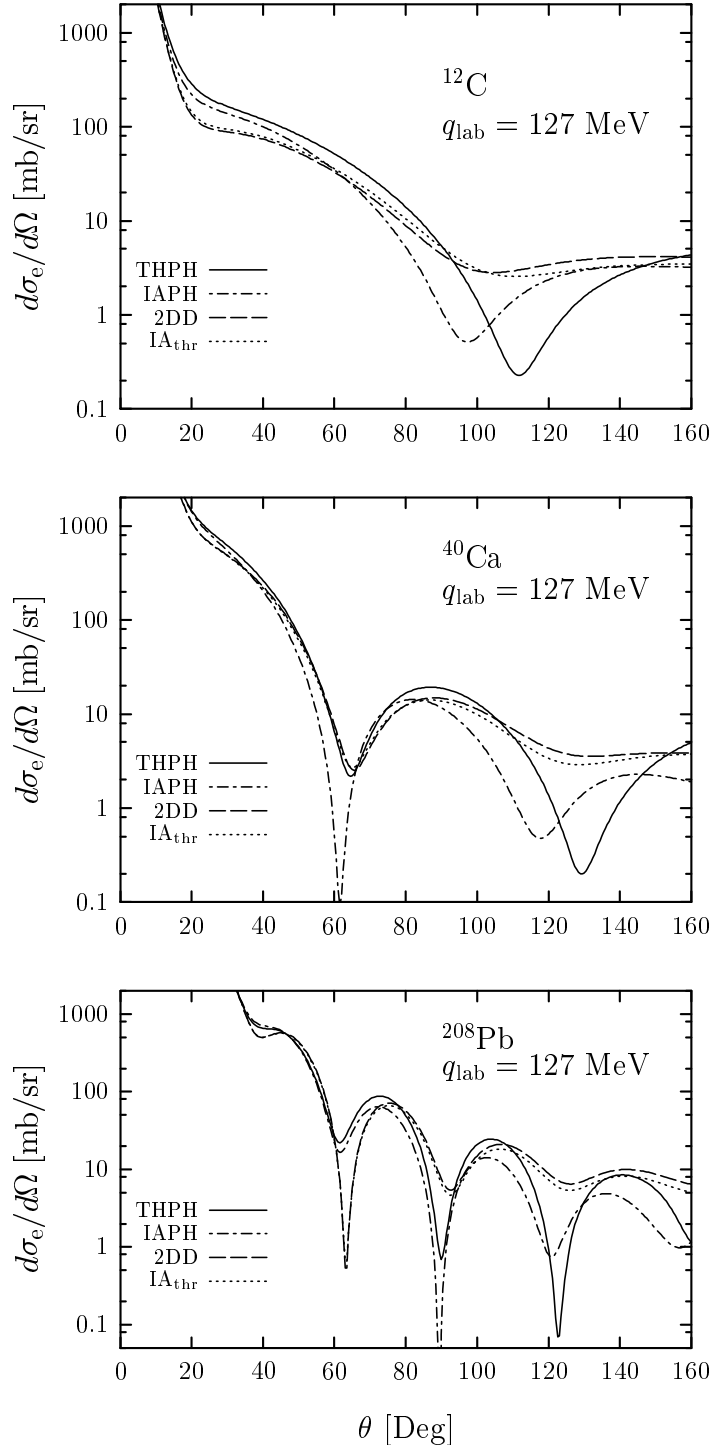


Figure 3: CM differential cross section for elastic scattering of  $q_{\text{lab}} = 127 \text{ MeV } K^-$  from  $^{12}\text{C}$ ,  $^{40}\text{Ca}$  and  $^{208}\text{Pb}$  with different antikaon selfenergies. The solid, dashed and dot-dashed lines have been obtained with  $\Pi^{\text{THPH}}$ ,  $\Pi^{\text{2DD}}$  and  $\Pi^{\text{IAPH}}$ , respectively, while the dotted line stands for the threshold IA, i.e.,  $\Pi(\sqrt{s}) = \Pi^{\text{IA}}|_{\sqrt{s}=m+M}$ .

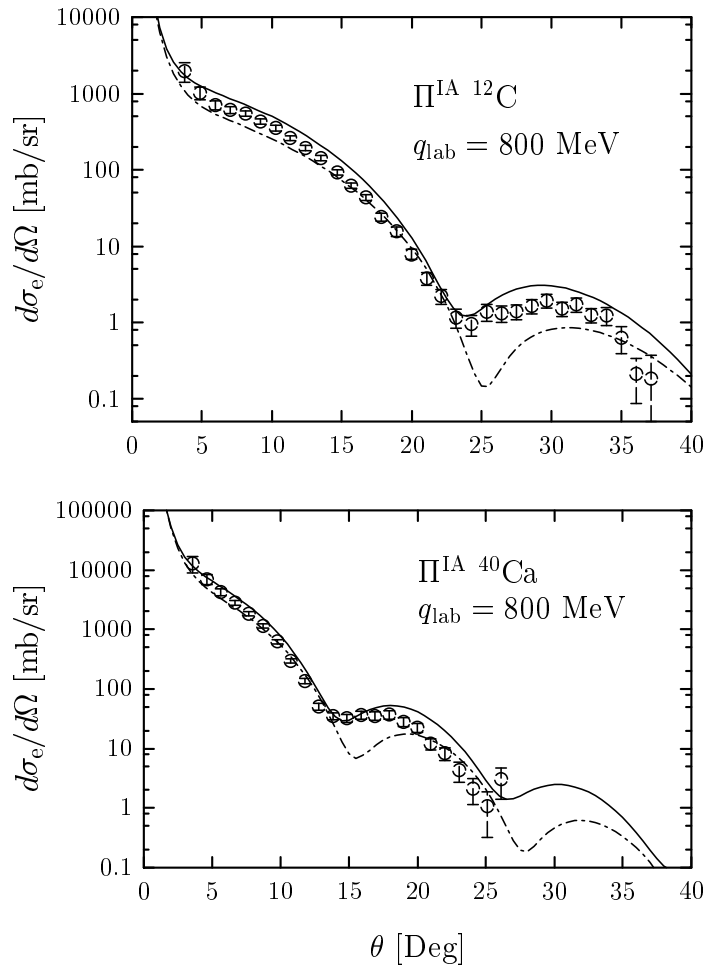


Figure 4: CM differential cross section for elastic scattering of  $q_{\text{lab}} = 800 \text{ MeV } K^-$  from  ${}^{12}\text{C}$  and  ${}^{40}\text{Ca}$ . Data are taken from Ref. [35] and the solid line has been obtained with IA selfenergy of Eq. (12) including  $s$ ,  $p$ ,  $d$  and  $f$ - waves. The amplitudes for these partial waves have been taken, for both isospin channels, from Ref. [36]. Finally the dashed line has been obtained with IA selfenergy, but including only  $s$  and  $p$  waves.

Potential	$^{12}\text{C}$			$^{40}\text{Ca}$			$^{208}\text{Pb}$		
	$\sigma_e$	$\sigma_{\text{react}}$	$\sigma_{\text{tot}}$	$\sigma_e$	$\sigma_{\text{react}}$	$\sigma_{\text{tot}}$	$\sigma_e$	$\sigma_{\text{react}}$	$\sigma_{\text{tot}}$
$\Pi^{\text{THPH}}$	444	501	945	1190	1201	2391	4345	4219	8564
$\Pi^{\text{2DD}}$	370	415	785	1064	1024	2088	4287	3667	7954
$\Pi^{\text{IAPH}}$	411	568	979	1029	1313	2342	4094	4363	8457
$\Pi^{\text{IA}} _{\sqrt{s}=m+M}$	380	420	800	1040	1043	2083	4264	3699	7963

Table 2: Strong integrated elastic, reaction and total cross sections (in mb) at  $q_{\text{lab}} = 127$  MeV, for all selfenergies and nuclei of Fig. 3.

$\Pi^{\text{2DD}}$ . The semiphenomenological  $\Pi^{\text{THPH}}$  selfenergy, has a stronger departure from a linear behaviour in density than  $\Pi^{\text{2DD}}$  (remember that the parameter  $\alpha$  is just 0.273), it has a smaller imaginary part (see Fig. 1 of Ref. [23]) and one might expect bigger differences with the IA model. This is what can be appreciated in Fig. 3. Results obtained with  $\Pi^{\text{THPH}}$  are clearly distinguishable from those obtained with any of the other three models also plotted in the figure. As a matter of example, for  $^{12}\text{C}$  in the region around  $\theta = 60^\circ$ , 2DD, IA and IAPH give similar elastic cross sections of about 33 mb/sr, whereas THPH gives about 52 mb/sr. This difference is appreciable and the cross sections are sizeable, order of tens of mb/sr, and thus it might be possible to measure such a difference at DAΦNE or KEK or in the future at the JHC. The discrepancies between the models are even bigger for larger angles, around the minimum of the THPH cross section (region  $110\text{--}130^\circ$ ), but there, the cross sections are smaller, of the order of 1 mb/sr, which makes harder to get the required statistics to see the effect. Besides, theoretical results in the neighborhood of a minimum are subject to more uncertainties. In calcium and around  $85^\circ$ , the 2DD, IA and IAPH models give elastic cross sections of around 14 mb/sr, while the THPH elastic cross section is about 19 mb/sr. In the region around the THPH minimum, the differences are larger, THPH (0.2 mb/sr), 2DD (3.5 mb/sr), IA (2.9 mb/sr) and IAPH (1.4 mb/sr), though the size of the cross sections is smaller. Similar conclusions can be drawn from the  $^{208}\text{Pb}$  results. In what respects to the integrated cross sections, compiled in Table 2, 2DD and IA give similar cross sections, though the IA reaction cross section always is slightly bigger, because the imaginary part of the  $B_0$  parameter in Eq. (16) is negative. The IAPH model always provides the biggest reaction cross sections, because its selfenergy has also the largest imaginary part among all models considered (see Fig. 1 of Ref. [23]). The numbers of the table indicate that one can easily differentiate two sets of models, i.e, 2DD and IA models from THPH and IAPH ones. Besides, measurements, with precisions of about 10%, of the reaction cross sections would disentangle between THPH and IAPH models.

Let us look now to the existing experimental  $K^-$ -nucleus scattering data. There exist data [35] on differential elastic cross sections for a  $K^-$  momentum of  $q_{\text{lab}} = 800$  MeV from  $^{12}\text{C}$  and  $^{40}\text{Ca}$ . In Fig. 4, we show the CM differential cross section for elastic scattering of  $q_{\text{lab}} = 800$  MeV  $K^-$  from  $^{12}\text{C}$  and  $^{40}\text{Ca}$  within the IA approximation and compare to the data of Ref. [35]. Two different approximations are shown. The solid

(dashed) line stands for the results obtained from an IA selfenergy  $\Pi^{IA}$  which includes up to  $f$ - ( $p$ -)waves. The isoscalar and isovector  $K^-$ -nucleon partial waves have been taken from Ref. [36], taking into account that the amplitudes ( ${}_I T_l^j$ ) given in that reference and those appearing in Eq. (13) are related by a factor  $p_{CM}$  (i.e.,  ${}_I T_l^j = {}_I f_l^j p_{CM}$ ), being  $p_{CM}$  the CM antikaon-nucleon momentum. We draw two main conclusions: i) The IA leads to a reasonable description of the data, what makes this region less sensitive to in nuclear medium effects. Indeed, calculations within the Glauber approximation provided an acceptable description of the data [37]. That reference also corroborates that the imaginary part of the  $K^-$ -nucleon scattering amplitude obtained from the  $K^-$ -nucleus scattering data is close to the value given in free space, though the real part of the forward scattering amplitude extracted from the scattering data on nuclei differs from the free space amplitude indicating some dropping of it at finite nuclear density. ii) The contribution of  $d$ - and  $f$ - waves, not included in the model of Refs. [9] and [24], is important. Besides, the model of Ref. [24] for the  $p$ -wave, though realistic near threshold, can not be safely extrapolated to momenta as high as 800 MeV.

For all of these, we refrain to present any result obtained from antikaon selfenergies tuned near threshold.

There also exist some data of integrated total cross sections from  $^{12}\text{C}$ , with the prescription discussed above of setting to zero the Coulombian phase shifts. At  $q_{\text{lab}} = 800$  and  $q_{\text{lab}} = 655$  MeV, the Ref. [38] gives  $338.2 \pm 2.2 \pm 7.2$  and  $306.0 \pm 3.7 \pm 7.0$ , (units of mb) respectively. The IA selfenergy, including up to  $f$ -waves, gives 345 mb at 800 MeV and 304 mb at 655 MeV. Thus we see again that the IA provides an acceptable description of data.

To finish, we also present results at an intermediate antikaon momentum ( $q_{\text{lab}} = 300$  MeV), despite the fact that there exist no data. For this momentum, calculations based on the IA shows that higher waves than the  $p$  one have a small/moderate contribution and therefore can be neglected in some approximations. Thus in Fig. 5 and Table 3, we compare again the THPH, 2DD and IAPH models for the antikaon selfenergy inside the nuclear medium, together with the IA results including up to the  $p$ -wave, or up to the  $d$ -wave (partial waves are taken from Ref. [36]). The first observation is that the 2DD model differs now more than for the 127 MeV momentum case, from the IA models. This is mainly due to the effect of  $p$ -wave in the latter ones. The second observation is that the semiphenomenological model THPH leads to a pattern clearly different than the rest of selfenergies, not only in the elastic differential cross section but also in the integrated ones compiled in Table 3. This is in principle good news, because then a scattering measurement in this region of antikaon momentum will be definitive to disentangle between this approach and the others considered in Fig. 5 and Table 3. However a word of caution must be said here,  $q_{\text{lab}} = 300$  MeV corresponds to a total CM antikaon-nucleon energy of about 1486 MeV. The  $s$ -wave part of the antikaon selfenergy of Ref. [9] is based on a model for the  $K^-$ -nucleon scattering in the free space that, though it is quite successful near threshold, predicts amplitudes for the isoscalar channel around 1486 MeV of total CM energy, with real parts which are in total disagreement (in sign and in size, see Ref. [39]) with the analysis of Ref. [36]. Thus, most probably one cannot trust the THPH model to describe the  $K^-$ -dynamics at this momentum. Indeed, there is no reason either to believe

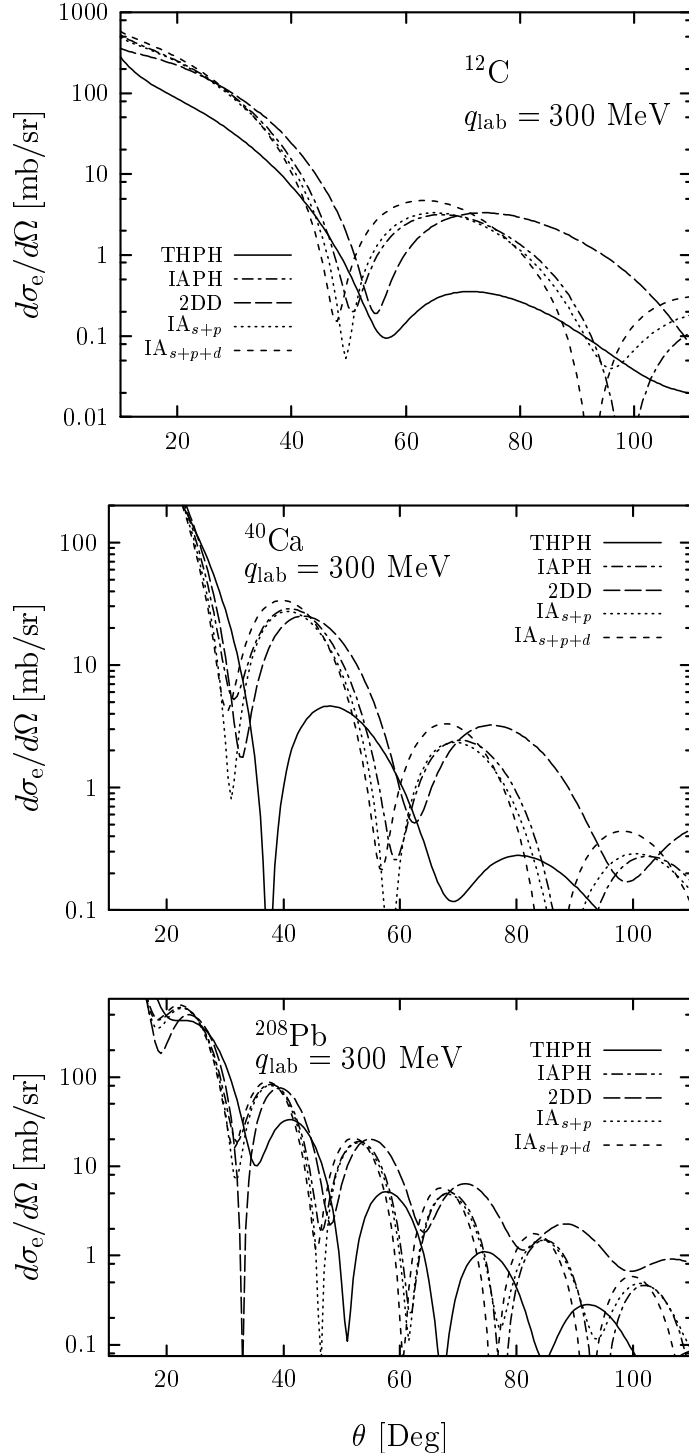


Figure 5: CM differential cross section for elastic scattering of  $q_{lab} = 300$  MeV  $K^-$  from  $^{12}C$ ,  $^{40}Ca$  and  $^{208}Pb$  with different antikaon selfenergies. The solid, long-dashed and dot-dashed lines have been obtained with  $\Pi^{THPH}$ ,  $\Pi^{2DD}$  and  $\Pi^{IAPH}$ , respectively, while the dotted and the short-dashed lines stand for the  $s + p$  and  $s + p + d$  IA selfenergies, respectively.

Potential	$^{12}\text{C}$			$^{40}\text{Ca}$			$^{208}\text{Pb}$		
	$\sigma_e$	$\sigma_{\text{react}}$	$\sigma_{\text{tot}}$	$\sigma_e$	$\sigma_{\text{react}}$	$\sigma_{\text{tot}}$	$\sigma_e$	$\sigma_{\text{react}}$	$\sigma_{\text{tot}}$
$\Pi^{\text{THPH}}$	71	250	321	242	572	814	1329	2074	3403
$\Pi^{\text{2DD}}$	252	312	564	545	737	1282	2057	2288	4345
$\Pi^{\text{IAPH}}$	250	374	624	613	858	1471	2115	2562	4677
$\Pi^{\text{IA}} _{s+p}$	248	384	632	615	874	1489	2148	2557	4705
$\Pi^{\text{IA}} _{s+p+d}$	278	406	684	653	913	1566	2195	2642	4837

Table 3: Strong integrated elastic, reaction and total cross sections (in mb) at  $q_{\text{lab}} = 300$  MeV, for all selfenergies and nuclei of Fig. 5.

more in the 2DD and IAPH models, and we believe that the more reliable predictions for  $q_{\text{lab}} = 300$  MeV are those based on the IA.

## Acknowledgments

We warmly thank E. Oset and A. Ramos for useful discussions. A.J. Melgarejo wishes to acknowledge a fellowship from the Plan Propio of the University of Granada. This research was supported by DGI and FEDER funds, under contract BFM2002-03218 and by the Junta de Andalucía.

## References

- [1] H. Tamura, plenary talk given at PANIC02, Osaka, Japan 2002.
- [2] N. Kaiser, P.B. Siegel and W. Weise, Nucl. Phys. **A594** (1995) 325.
- [3] N. Kaiser, P.B. Siegel and W. Weise, Phys. Lett. **B362** (1995) 23.
- [4] N. Kaiser, T. Waas and W. Weise, Nucl. Phys. **A612** (1997) 297.
- [5] E. Oset and A. Ramos, Nucl. Phys. **A635** (1998) 99.
- [6] J. A. Oller and Ulf. G. Meißner, Phys. Lett. **500** (2001) 263.
- [7] M. F. M. Lutz and E. E. Kolomeitsev, Nucl. Phys. **A 700** (2002) 193.
- [8] C. García-Recio, J. Nieves, E. Ruiz Arriola and M.J. Vicente Vacas, Talk given in QNP2002, Jülich, Germany, June 2002, nucl-th/0209053; *ibidem* Talk given in PANIC02, Osaka, Japan 2002.
- [9] A. Ramos and E. Oset, Nucl. Phys. **A671** (2000) 481.

- [10] J.A. Oller and E. Oset, Nucl. Phys. **A620** (1997) 438; J.A. Oller, E. Oset and J.R. Peláez, Phys. Rev. Lett. **80** (1998) 3452; *ibidem*, Phys. Rev. **D59** (1991) 074001.
- [11] J. Nieves and E. Ruiz Arriola, Phys. Lett. **B455** (1999) 30; *ibidem*, Nucl. Phys. **A679** (2000) 57.
- [12] J. Nieves and E. Ruiz Arriola, Phys. Rev. **D64** (2001) 116008.
- [13] T. Inoue, E. Oset and M. J. Vicente Vacas, Phys. Rev. **C65** (2002) 035204.
- [14] C.J.Batty, E. Friedman and A. Gal, Phys. Rep. **287** (1997) 385.
- [15] E. Friedman, A. Gal and C.J. Batty, Phys. Lett. **B308** (1993) 6.
- [16] E. Friedman, A. Gal and C.J. Batty, Nucl. Phys. **A579** (1994) 518.
- [17] E. Friedman, A. Gal, J. Mares and A. Cieply, Phys. Rev. **C60** (1999) 024314.
- [18] E. Friedman and A. Gal, Phys. Lett. **B459** (1999) 43.
- [19] M. F. M. Lutz, Phys. Lett. **B426** (1998) 12-20; and *nucl-th/9802033*.
- [20] J. Schaffner-Bielich, V. Koch and M. Effenberger, Nucl. Phys. **A669** (2000) 153.
- [21] L. Tolos, A. Ramos and A. Polls, Phys. Rev. **C65** (2002) 054907.
- [22] S. Hirenzaki, Y. Okumura, H. Toki, E. Oset and A. Ramos, Phys. Rev. **C61** (2000) 055205.
- [23] A. Baca, C. García-Recio and J. Nieves, Nucl. Phys. **A673** (2000) 335.
- [24] C. García-Recio, J. Nieves, E. Oset and A. Ramos, Nucl. Phys. **A703** (2002) 271.
- [25] D.B. Kaplan and A. E. Nelson, Phys. Lett. **B175** (1986) 57.
- [26] J. Nieves, E. Oset and C. García-Recio, Nucl. Phys. **A554** (1993) 554.
- [27] E. Oset and L.L. Salcedo, J. Comput. Phys. **57** (1985) 55.
- [28] A. Galindo and P. Pascual, “Quantum Mechanics” (Springer, Berlin 1991)
- [29] C.W. de Jager, H. de Vries and C. de Vries, At. Data and Nucl. Data Tables **14** (1974) 479; **36** (1987) 495.
- [30] J.W. Negele and D. Vautherin, Phys. Rev. **C11** (1975) 1031 and references therein.
- [31] D. Jido, E. Oset and A. Ramos, Phys. Rev. **C** in print, *nucl-th/0208010*.
- [32] J. Nieves, E. Oset and C. García-Recio, Nucl. Phys. **A554** (1993) 509.
- [33] J. Taylor, Scattering Theory (J. Wiley & Sons, 1972)
- [34] A. D. Martin, Nucl. Phys. **B179** (1981) 33.

- [35] D. Marlow, et al., Phys. Rev. **C25** (1982) 2619.
- [36] G.P. Gopal et al., Nucl. Phys. **B119** (1977) 362.
- [37] A. Sibirtsev and W. Cassing, Phys. Rev. **C61** (2000) 057601.
- [38] D.V. Bugg, et al., Phys. Rev. **168** (1968) 1466.
- [39] E. Oset, A. Ramos and C. Bennhold, Phys. Lett. **B522** (2002) 260.